JOURNAL OF GUIDANCE, CONTROL, AND DYNAMICS
Vol. 20, No. 6, November–December 1997

Nonlinear Viscoelastic-Plastic Mechanisms-Based Model of an Electrorheological Damper

Gopalakrishna M. Kamath and Norman M. Wereley
University of Maryland, College Park, Maryland 20742

A combined theoretical and experimental study of an electrorheological (ER) fluid damper is presented. An ER dashpot damper was built and its dynamic characteristics tested at different electric field strengths and varying displacement amplitudes. A nonlinear model is proposed that describes the dynamic behavior of the damper. The model is constructed using a nonlinear combination of linear mechanisms. The mechanisms are chosen based on the experimentally observed preyield and postyield characteristics of the damper behavior. The model parameters are estimated from the experimental hysteresis data. The force vs displacement and force vs velocity hysteresis cycles are then reconstructed using these estimated parameters. The results show that the model captures the nonlinear damper behavior quite accurately. The importance of the various components in the model is illustrated.

I. Introduction

THERE has been an increased emphasis on reducing the number of movable parts in helicopter rotor hubs to prolong life and reduce maintenance costs. This has led to the development of advanced rotor systems such as hingeless and bearingless rotors. These soft in-plane rotor systems tend to suffer from aeromechanical instabilities such as air and ground resonances.[1] These instabilities can be mitigated by augmenting the lag mode damping in these rotors. Hydraulic dampers and elastomeric dampers, which use viscoelastic materials, are currently being used for this purpose. However, elastomers are highly nonlinear materials whose properties are dependent on both frequency and temperature. Their nonlinear dual-frequency behavior has been shown to reduce damping and thus cause limit cycle oscillations at low amplitudes.[2] The storage modulus (stiffness) and loss modulus (damping) of elastomers are displacement dependent, and the loss modulus is typically inadequate for small displacements. To overcome this shortcoming, dampers have been proposed using elastomers in combination with hydraulic fluids, so that these dampers have storage and loss moduli that remain relatively constant with amplitude.[3,4] But for accurate blade tracking, the damper for each blade has to be matched exactly. Moreover, damping augmentation is required only in certain flight regimes. These specifications can be met using a damper with adaptive properties. Controllable fluid dampers are an attractive choice for meeting these blade tracking and lag mode damping augmentation specifications in advanced rotor systems. One of the impediments in the application of these dampers is the lack of a suitable model to predict their dynamic behavior. Helicopter rotor system dynamics and stability are sensitive to the dynamic characteristics of the lag mode damper. Hence, it is important to accurately model damper behavior under harmonic excitation for variable conditions of load, damper shaft stroke and velocity, and frequency. The model should contain a small number of degrees of freedom or states, so as not to severely degrade the execution times of comprehensive helicopter aeroelastic codes, such as the University of Maryland Advanced Rotorcraft Code (UMARC).[5] This paper presents a theoretical and experimental study of electrorheological (ER) fluid dampers that serves as a step toward this goal.

Controllable fluids such as ER and magnetorheological (MR) fluids belong to the class of active materials that have the unique ability to change dynamic yield stress when acted upon by an electric or magnetic field, while maintaining viscosity relatively constant. ER fluid applications have so far outnumbered those of MR fluids primarily due to the wider commercial availability of ER fluids.[6–8]

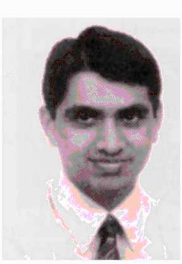

Gopalakrishna M. Kamath is a doctoral candidate in the Department of Aerospace Engineering at the University of Maryland at College Park. He graduated with a B.Tech. in Aerospace Engineering from the Indian Institute of Technology, Madras, India. He earned his M.S. in 1994 from the University of Maryland at College Park. His dissertation is focused on helicopter rotor stability augmentation strategies using electrorheological and magnetorheological fluid-based semiactive actuators. He is a Student Member of AIAA and is a recipient of the Vertical Flight Foundation Fellowship and Minta Martin Fellowship.

Norman M. Wereley is an Assistant Professor in the Department of Aerospace Engineering at the University of Maryland at College Park. He holds a B.Eng. (Honors) in Mechanical Engineering from McGill University in Montreal, Canada, and an M.S. and a Ph.D. in Aeronautics and Astronautics from the Massachusetts Institute of Technology. He joined the Alfred Gessow Rotorcraft Center in 1993, and his research interests are in dynamics and control of smart structures, with emphasis on active and passive vibration damping control applied to rotorcraft systems. He is a Member of AIAA and an Associate Editor for the *Journal of Intelligent Material Systems and Structures* and serves on the editorial board of the *Journal of Smart Materials and Structures*.

Presented as Paper 97-0359 at the AIAA 35th Aerospace Sciences Meeting, Reno, NV, Jan. 6–9, 1997; received Jan. 27, 1997; revision received July 20, 1997; accepted for publication July 31, 1997.

MR fluids have captured the attention of researchers only recently. MR fluids have an order of magnitude higher dynamic yield stress as compared to ER fluids and a broader operational temperature range.[9] This paper focuses primarily on a mechanisms-based approach for modeling ER fluid damper behavior. But ER and MR fluids exhibit qualitatively similar rheological characteristics,[10] so that the model can be applied to MR fluid dampers as well. The model uses linear mechanisms in conjunction with nonlinear shape functions to model the various nonlinear effects, such as transition at yield and coulomb friction effects at low amplitudes. This paper also describes the experiments that were conducted to support and validate the mechanisms-based ER damper model. The results show that the model captures the nonlinear effects quite accurately and, thus, would provide a valuable tool in the design and performance prediction of systems incorporating controllable fluids.

ER fluids behave like simple viscous fluids in the absence of an electric field, and their behavior can be described by the Newtonian shear model. When an electric field is applied, the fluid exhibits a yield phenomenon wherein the material does not flow until the critical yield stress value is exceeded. This yield stress value nominally increases as a quadratic function of the applied electric field. An idealized model to describe this yield phenomenon is the Bingham plastic model. This model is a good approximation for the postyield behavior, and can be used as a starting point for damper design.[11–13] The Bingham plastic model can be used for quasisteady loading[11] and dynamic loading.[12] But under dynamic loading conditions, the preyield behavior, which is ignored in the Bingham plastic model, also plays an important role in determining the overall dynamic characteristics of the damper. Frequency and amplitude of excitation must also be considered under conditions of dynamic loading, which are not accounted for in the Bingham plastic model.

Various models have been proposed to describe the dynamic properties of ER fluids and ER fluid dampers. Gamota et al.[14] proposed a model based on the Fourier analysis of ER fluid stress response to a sinusoidal shear deformation of amplitude 0.5 and frequency 10 Hz as the material was subjected to increasing electric field strengths. The experimental studies on which this model was based provided valuable insight into the dynamic behavior of these materials.[15,16] The authors proposed a nonlinear viscoelastic–plastic model, which described the preyield and the postyield characteristics of an ER fluid using a nonlinear network of linear viscoelastic and viscous elements.[17,18] The models of Refs. 14–18 are strictly for describing ER material behavior. These models depend only on the material properties.

There are also models that describe controllable fluid damper behavior. Apart from the fluid properties, the modeling of a damper involves geometry-dependent properties such as the damper size and other built up damper effects due to rod seals and bearings. Stanway et al.[19] proposed using a coulomb element in parallel with a dashpot element. The element parameters were estimated using a nonlinear filtering algorithm. Ehrgott and Masri[20] conducted experiments with a dynamic testing device incorporating an ER fluid. The device response was simulated using a nonparametric identification method based on Chebyshev polynomials. Lou et al.[21] used the Bingham plastic model with factors to account for the frequency effects and conducted a parametric study to evaluate the performance of different configurations. Spencer et al.[22] proposed the Bouc–Wen model to describe MR damper behavior. The current authors extended the nonlinear viscoelastic–plastic fluid model to describe the behavior of a mixed mode type of damper.[23,24] The frequency response of a mass-spring-ER damper system was shown to be very close to that of a proportional coulomb and viscously damped system.[24] Makris et al.[25] developed a phenomenological elastic–plastic model to account for the preyield and postyield behavior and used it in conjunction with a neural network to predict the nonlinear behavior.

This paper presents a combined experimental and theoretical study of an ER fluid damper. A mixed mode, moving electrode ER damper was built and tested for different field strengths and excitation amplitudes. An augmented six-parameter model is introduced that simulates both the force–displacement and the force–velocity hysteresis cycles, which represents an extension to the four-parameter viscoelastic–plastic ER flow model from Ref. 18 for predicting damper behavior. The model uses linear mechanisms, and the nonlinearities are captured using smooth nonlinear shape functions. This makes the model more amenable to numerical implementation than directly using nonlinear mechanisms such as those with slope discontinuities. The linear mechanisms are based on the observed phenomenology of the dampers and contain only a few parameters that can be easily estimated. The augmented six-parameter model accurately captures the nonlinear coulomb effects and the effects of fluid inertia that were not entirely accounted for by the four-parameter viscoelastic–plastic model used in Refs. 23 and 24.

II. ER Damper Experiments

A mixed mode moving electrode ER damper was designed and built for this study. In this damper configuration, one electrode moves relative to the other. The resisting force of the damper is then a sum of the viscous drag due to the relative motion between the electrodes and the pressure drag force created as a reaction to the ER fluid being forced through the electrode gap. A sketch of the ER damper is shown in Fig. 1. The outer shell and the piston head are made of aluminum, so that they also serve as the two electrodes. In the damper used for this study, the electrode gap was chosen to be 0.1 in. The damper has a nominal stroke of 2 in. peak-to-peak. The other dimensions shown in Fig. 1 were then determined using the quasisteady Bingham plastic model equations for a moving electrode damper.[11] The ER fluid used was the VersaFlo ER-100 manufactured by Lord Corporation. O-ring seals were used to contain the fluid inside the damper, and linear bearings were used to align the inner electrode with the outer shell. A steel frame was built

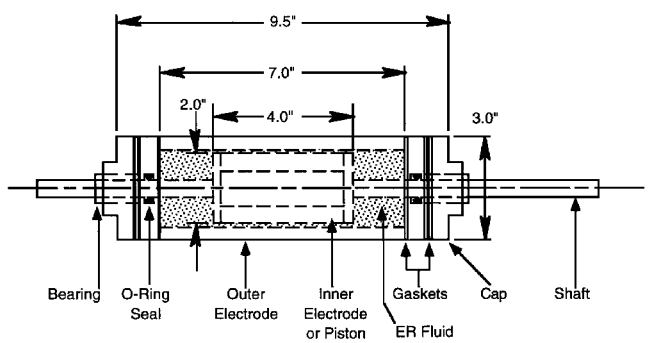

Fig. 1 Sketch of the mixed mode moving electrode ER fluid damper.

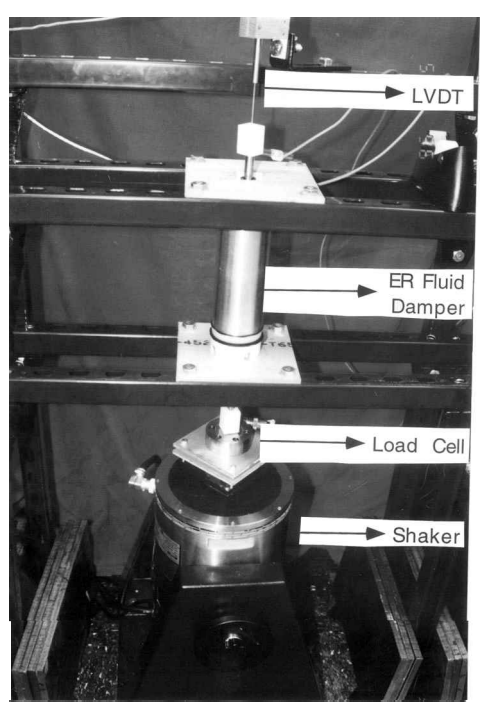

Fig. 2 Experimental setup for dynamic testing of ER fluid dampers.

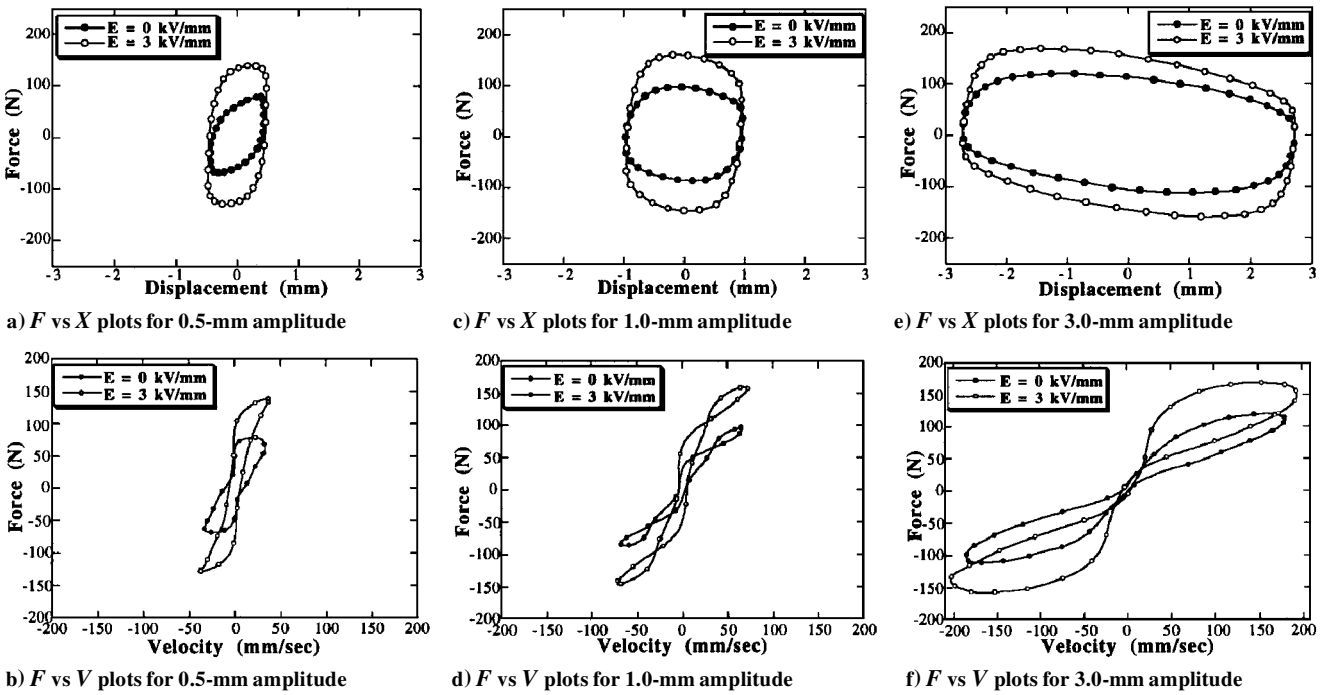

a) F vs X plots for 0.5-mm amplitude
c) F vs X plots for 1.0-mm amplitude
e) F vs X plots for 3.0-mm amplitude
b) F vs V plots for 0.5-mm amplitude
d) F vs V plots for 1.0-mm amplitude
f) F vs V plots for 3.0-mm amplitude

Fig. 3 Sample set of experimental hysteresis data for different displacement amplitudes and field strengths.

to support the outer shell, and the shaft with the piston was free to be connected to the shaker. The experimental setup for the dynamic test measurements is shown in Fig. 2. A Brüel Kjær 4801T shaker was used to excite the shaft, which is connected to the piston. The shaker had a maximum force output of 85 lb with a displacement range of 0.5 in. peak-to-peak. A Sensotec load cell with 100-lb range was mounted between the shaft and the shaker to measure the force input to the damper. A Schaevitz linear variable differential transformer (LVDT) measured the shaft displacement. The time history signals from the load cell and the LVDT were recorded using a Hewlett Packard 35665A spectrum analyzer. A sinusoidal signal with a frequency of 10 Hz was used to drive the shaker. The force levels and, hence, the displacement levels were changed by varying the gain on the shaker amplifier. The measurements were made for various displacement amplitudes, and each of these measurements was repeated for varying electric field strengths. The readings from the load cell were plotted against the LVDT measurements to generate the force vs displacement hysteresis cycles. The periodic displacement data measured by the LVDT were first filtered to remove the high-frequency noise components using a simple Fourier decomposition. The velocity time histories of the damper were then calculated from the respective displacement data using a fourth-order central difference scheme.

III. Experimental Results

A representative set of experimental hysteresis data is plotted in Fig. 3. The plot shows the force vs displacement (F vs X) and the force vs velocity (F vs V) hysteresis cycles for the two extreme values of electric field, 0 and 3 kV/mm, and for three displacement amplitudes, 0.5, 1.0, and 3.0 mm.

A. Effect of Electric Field

It can be seen from Figs. 3a, 3c, and 3e that, as the applied electric field is increased, the amount of damping that is represented by the area enclosed by the force vs displacement hysteresis cycle also increases. The Bingham plastic-like behavior of ER materials can be seen in the force vs velocity hysteresis cycles (Figs. 3b, 3d, and 3f). If a line is drawn approximately through the center of the F vs V cycles, a curve is obtained that is at best reminiscent of the force vs velocity (or shear stress vs strain rate) curves for Bingham plastic materials (Fig. 4). It can also be seen that the idealized yield force increases from approximately 20 N for no applied field (Fig. 4a) to about 50 N for an electric field of 3 kV/mm (Fig. 4b).

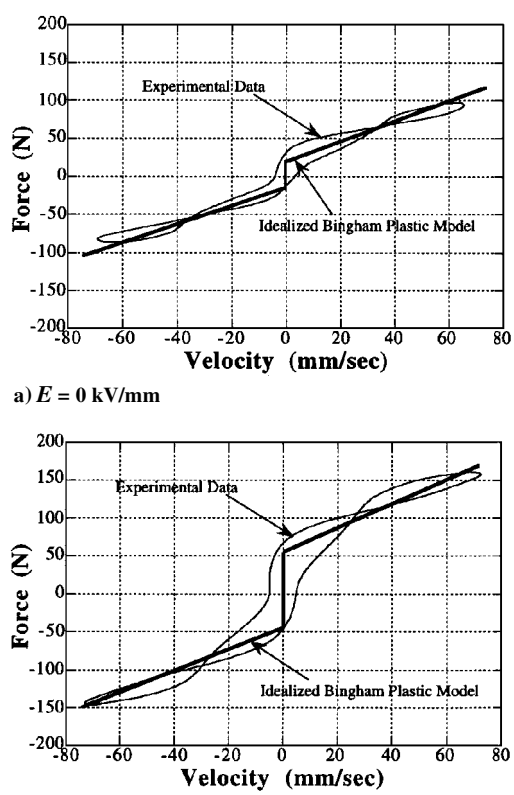

a) E = 0 kV/mm
b) E = 3 kV/mm

Fig. 4 Comparison of force vs velocity hysteresis cycles with the idealized Bingham plastic model for a displacement amplitude of 1.0 mm for applied electric fields.

B. Effect of Displacement Amplitude

The three amplitudes for which the hysteresis plots are shown in Fig. 3 were chosen to nominally represent the three rheological domains: the preyield, yield, and postyield regions of the ER fluid behavior. The displacement and velocity time histories for the three displacements and an electric field of 3.0 kV/mm are shown in Fig. 5. The coulomb friction-like behavior is more pronounced for low amplitudes, and as the amplitude is increased, the displacement

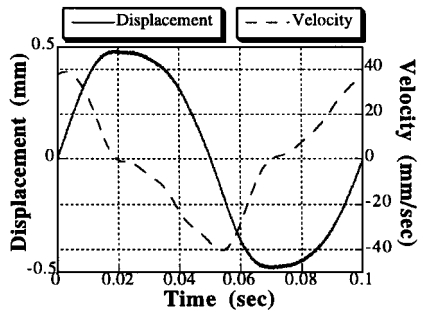

a) 0.5-mm amplitude

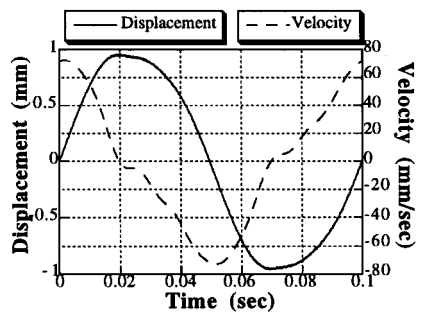

b) 1.0-mm amplitude

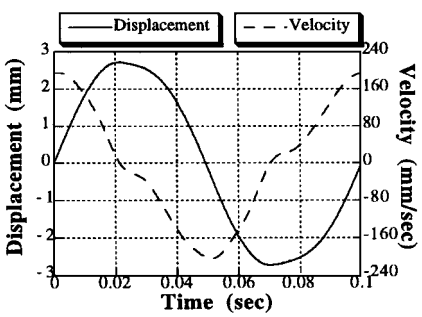

c) 3.0-mm amplitude

Fig. 5 Displacement and velocity time histories for $E = 3.0$ kV/mm and different displacement amplitudes.

time histories show a more sinusoidal behavior. The nature of these time histories is similar to those obtained by Stanway et al.[19] The differences in behavior through these three domains are manifested in a more obvious way in the F vs V hysteresis cycles and in a subtle way in the F vs X hysteresis cycles, shown in Fig. 3. For an amplitude of 0.5 mm (Fig. 3b), which is the preyield phase, the F vs V hysteresis cycles form a single loop traversing in an anticlockwise direction (the directions discussed are not obvious from the hysteresis plots and were determined from the raw experimental data), which is indicative of a viscoelastic nature. As the amplitude is increased to 1.0 mm (Fig. 3d), two additional loops appear at the extremities in which the direction is clockwise. This is indicative of a viscous nature with fluid inertia effects. Thus, this curve shows the transition at yield from a viscoelastic behavior to a viscous behavior. As the amplitude is increased further (Fig. 3f), the inner loop shrinks for $E = 3$ kV/mm and totally disappears for $E = 0$ kV/mm. This shows that the fluid as fully yielded, and its viscous nature dominates the damper behavior. The elliptical nature of the F vs X hysteresis cycles (Fig. 3e) also suggests this viscous behavior, and the slight negative inclination of the ellipses demonstrates the effects of fluid inertia.

C. Energy Dissipation and Equivalent Damping

The energy dissipated by a damper over one vibration cycle is a measure of its damping capacity. This is given by the area enclosed within the F vs X hysteresis cycle, which is given by the integral

$$U = \oint F\,\mathrm{d}x = \int_0^{2\pi/\Omega} F v\,\mathrm{d}t \tag{1}$$

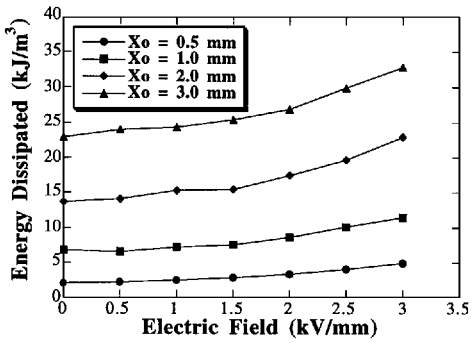

Fig. 6 Variation of dissipated energy with electric field for different displacement amplitudes.

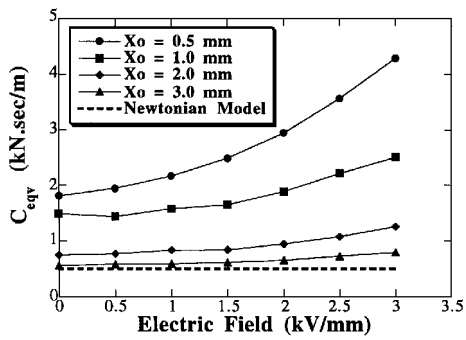

Fig. 7 Variation of equivalent damping coefficient C_{eqv} with electric field for different displacement amplitudes with the Newtonian model as the baseline value.

where Ω is the excitation frequency and v is the damper shaft velocity. Using the experimental data and integrating numerically, the dissipated energies were calculated for different field strengths and displacement amplitudes. To measure the efficiency of a controllable fluid damper, it is important to know the amount of damping achieved for a unit volume of active fluid. In an ER fluid damper configuration such as the one used in this study, the active fluid volume is the volume of fluid contained in the annular region between the two electrodes. Thus, for comparison purposes, it is more meaningful to calculate the dissipated energy per unit active fluid volume. These values were calculated and are plotted in Fig. 6. The dissipated energy appears to increase as a quadratic function of the electric field.

To compare the damping performance of a controllable fluid damper with that of a conventional viscous dashpot damper, an equivalent damping coefficient can be determined for the former by equating the energies dissipated in the two cases. Thus,

$$C_{\mathrm{eqv}} = \frac{U}{\pi \Omega X_0^2} \tag{2}$$

where U is the dissipated energy as given by Eq. (1) and X_0 is the displacement amplitude. The equivalent damping coefficients for different sets of data are plotted in Fig. 7. It can be seen that for low amplitudes, where the fluid is in the preyield phase, the value of C_{eqv} rises more rapidly with increase in electric field than for high amplitudes, where the fluid is in the postyield phase. Thus, to exploit the adaptivity of the controllable fluid damper, the dampers have to be operated close to the yield point. For high amplitudes, the C_{eqv} curve tends to flatten to a horizontal line (zero adaptivity) with the C_{eqv} value equal to that of the zero field case, which is the Newtonian behavior. The dotted line represents the C_{eqv} value calculated for the zero-field case using a simple Newtonian model, as explained in Ref. 11.

IV. Augmented Six-Parameter Damper Model

The experimental results discussed in the preceding section offer a good understanding of the phenomenology of an ER damper. There are two distinct rheological domains over which the dampers

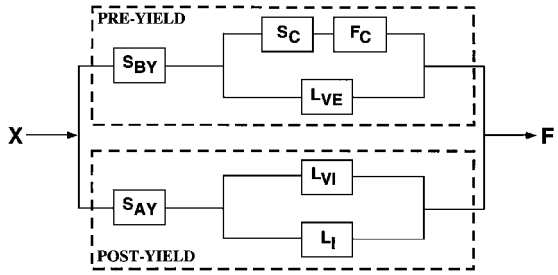

Fig. 8 Schematic of the augmented six-parameter model network for ER fluid dampers.

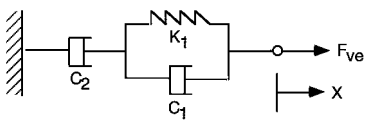

a) Viscoelastic mechanism L_{ve} in the preyield branch of the model

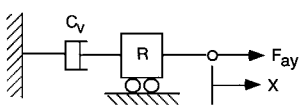

b) Viscous mechanism L_{vi} and the inertial mechanism L_i in the postyield branch of the model

Fig. 9 Mechanisms used in the model.

operate: the preyield and the postyield regions.[10] The preyield region is characterized by a strong viscoelastic nature and also exhibits some stiction properties. The coulomb-like stiction effects are contributed in different measures by the ER fluid and the damper components such as the dynamic rod seals. As the amplitude increases, the stiction effects appear to be less significant. The postyield region shows a dominant viscous behavior, where the fluid inertia effects come into play. The stiction and inertia effects are more apparent in the force vs velocity hysteresis data. The yield point separating the two rheological domains varies as a function of the electric field and the displacement amplitude. The overall behavior of the ER damper, thus, can be simulated by choosing the appropriate linear shear mechanisms for the two regions and then combining them to capture the transition between the two regions. A schematic of the network that accomplishes this is shown in Fig. 8. The network is similar to a control system block diagram and establishes a relation between the damper shaft displacement X and its derivatives, which is assumed to be the input and the damper force output F. One branch of the network comprises the preyield components, whereas the other branch contains the postyield components. The augmented six-parameter model describes not only the force vs displacement data but also the force vs velocity data.

A. Preyield Mechanisms

The three-parameter fluid model shown in Fig. 9a is used as the mechanical analog for the viscoelastic behavior in the preyield region. This is represented by the linear operator L_{ve} in the model network. The force–displacement differential equation of the viscoelastic analog in Fig. 9a is given in the time domain by

$$F_{ve} + p_1 \dot{F}_{ve} = q_1 \dot{X} + q_2 \ddot{X} \tag{3}$$

where F_{ve} is the viscoelastic component of the damper force and

$$p_1 = \frac{C_1 + C_2}{K_1}, \qquad q_1 = C_2, \qquad q_2 = \frac{C_1 C_2}{K_1}$$

If a sinusoidal excitation is assumed, then the differential equation, Eq. (3), can be written in the frequency domain as

$$F_{ve} = G^* X \tag{4}$$

where G^* is the complex shear coefficient,

$$G^* = G' + jG'', \qquad j = \sqrt{-1}$$

and

$$G' = \frac{K_1 C_2^2 \Omega^2}{K_1^2 + (C_1 + C_2)^2 \Omega^2} \tag{5}$$

$$G'' = \frac{(C_1 + C_2)\, C_1 C_2 \Omega^3 + K_1^2 C_2 \Omega}{K_1^2 + (C_1 + C_2)^2 \Omega^2} \tag{6}$$

where Ω is the excitation frequency. The stiction effects seen in the damper behavior at low velocities are described using the parameter F_c and the shape function S_c, which has been chosen as

$$S_c = \tfrac{1}{2}\{\tanh(\dot{X}/4\epsilon_c)\} \tag{7}$$

where $\dot{X}$ is the damper velocity and ϵ_c is the smoothening factor that ensures smooth transition from the negative to positive velocities and vice versa. The parameter ϵ_c was chosen a priori based on the extent of stiction effects observed in the force vs velocity hysteresis data. The factor of four is included in the shape function so that for $0 < \epsilon_c < 1$, the transition between the extremities of the hyperbolic tangent function occurs to the full extent and at a reasonable rate, represented by the slope of the function at the origin. Thus, the preyield force component is given by

$$F_{by} = F_{ve} + S_c F_c \tag{8}$$

where F_{ve} is given by Eq. (4).

The nonlinear shape function S_{by} is the preyield switching function, which along with S_{ay} effects the smooth transition from the preyield phase to the postyield phase. The functions S_{by} and S_{ay} are dependent on a yield parameter α_y that is chosen during the estimation process. The parameter α_y represents the yield transition point in a dynamic cycle and varies with the electric field and the displacement amplitude. The preyield shape function is given by

$$S_{by} = \tfrac{1}{2}\{1 - \tanh[(\alpha - \alpha_y)/4\epsilon_y]\} \tag{9}$$

where α is the damper shaft velocity nondimensionalized with respect to the amplitude and ϵ_y is a smoothening parameter and is chosen to have a constant value of 0.1. Because the shape functions perform the task of switching on and off the different mechanisms, the parameter F_c appears only at low velocities and is almost ineffective at high velocities, thus producing a stick–slip-type motion rather than a motion with a constant coefficient of friction.

B. Postyield Mechanisms

The postyield branch of the network consists of the viscous mechanism L_{vi} and the inertial component L_i. These components can be combined and represented as shown in Fig. 9b. Thus, the postyield force component is given by

$$F_{ay} = C_v \dot{X} + R\ddot{X} \tag{10}$$

S_{ay} is similar to the shape function S_{by}, where S_{ay} acts as a switching function to turn on the postyield mechanism when the damper crosses the yield point. It has been chosen as

$$S_{ay} = \tfrac{1}{2}\{1 + \tanh[(\alpha - \alpha_y)/4\epsilon_y]\} \tag{11}$$

C. Augmented Model

For a sinusoidal displacement input, the damper force output as given by the augmented six-parameter damper model is written as

$$F = S_{by} F_{by} + S_{ay} F_{ay} \tag{12}$$

where F_{by}, S_{by}, F_{ay}, and S_{ay} are given by Eqs. (8), (9), (10), and (11), respectively. Thus, rather than using nonlinear elements, the augmented model takes the novel approach of using linear mechanisms in conjunction with nonlinear shape functions. Moreover, the mechanisms chosen, the type of shape functions, and the structure of the model network are based heavily on the experimentally observed phenomenology of the damper behavior.

D. System Identification

Having established the model structure and the model components, the parameters in the model need to be identified. Because the

parameters ϵ_c, ϵ_y, and α_y are chosen a priori, the only unknown parameters are the viscoelastic parameters C_1, C_2, and K_1; the viscous parameter C_v; the inertial parameter R; and the stiction parameter F_c. The model uses the displacement as an input, calculates the velocities and accelerations needed for the model, and then gives the total force, given by Eq. (12), as the output. Thus, the six parameters are estimated on the basis of minimizing the error between this force output F and the actual force F_m obtained from experimental measurements. The error in the model is represented by the objective function J given by

$$J = \sum_{i=1}^{N} \left(F_i - F_{m_i}\right)^2 \tag{13}$$

where N is the number of data points for each hysteresis cycle, F is the force predicted by the model, and F_m is the experimentally measured force. To obtain physically meaningful results, the parameters are constrained to have positive values. The optimization was done with Design Optimization Tools (DOT),[26] which uses the Broyden–Fletcher–Goldfarb–Shanno algorithm to minimize the objective function in Eq. (13). The parameter α_y was manually chosen such that the objective function reached a minimum.

E. Results

Using the parameters estimated from the system identification process, the force vs displacement and the force vs velocity hysteresis cycles were reconstructed and compared with the experimental data. For the sample data set shown in Fig. 3, the reconstructed hysteresis cycles are shown in Figs. 10 and 11. Figures 10 and 11 show the reconstructed hysteresis cycles for different displacement amplitudes for $E = 0$ and 3 kV/mm, respectively. The plots show that the model accurately captures the nuances of the experimental data.

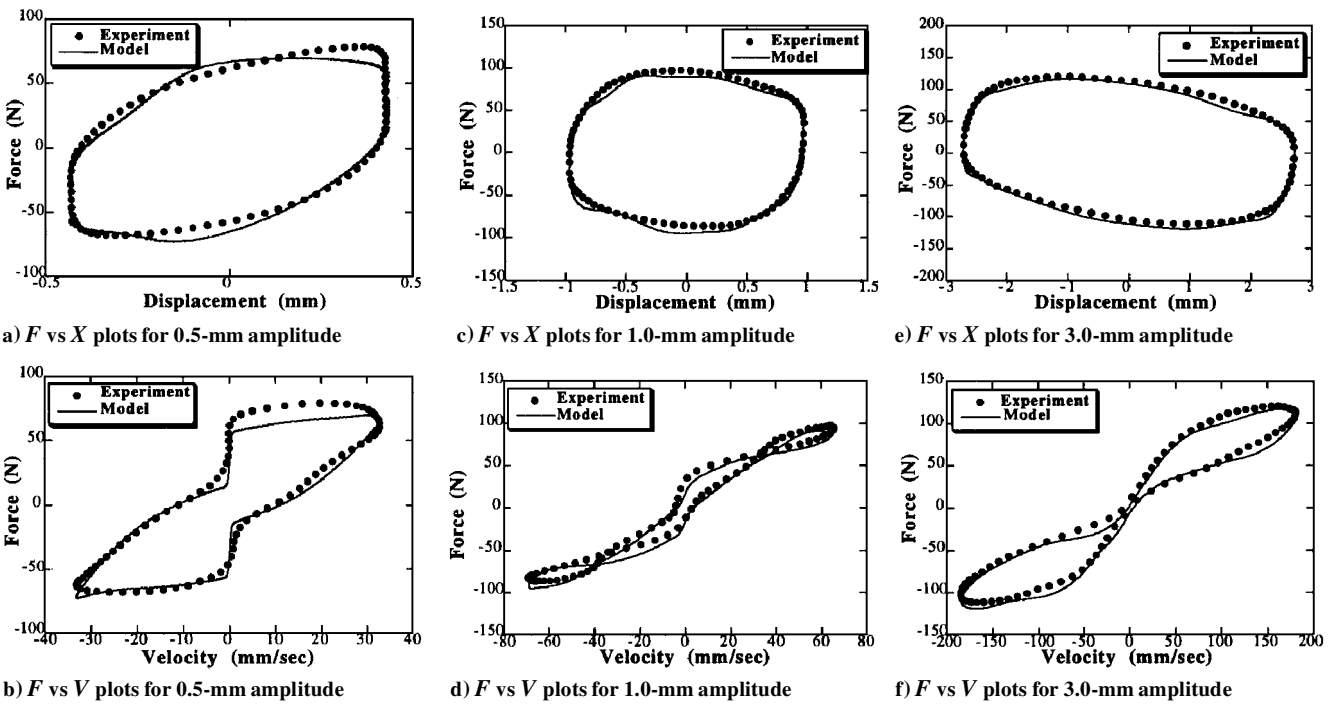

a) F vs X plots for 0.5-mm amplitude
c) F vs X plots for 1.0-mm amplitude
e) F vs X plots for 3.0-mm amplitude
b) F vs V plots for 0.5-mm amplitude
d) F vs V plots for 1.0-mm amplitude
f) F vs V plots for 3.0-mm amplitude

Fig. 10 Comparison of hysteresis cycles from estimated parameters with experimental hysteresis data for $E = 0$ kV/mm.

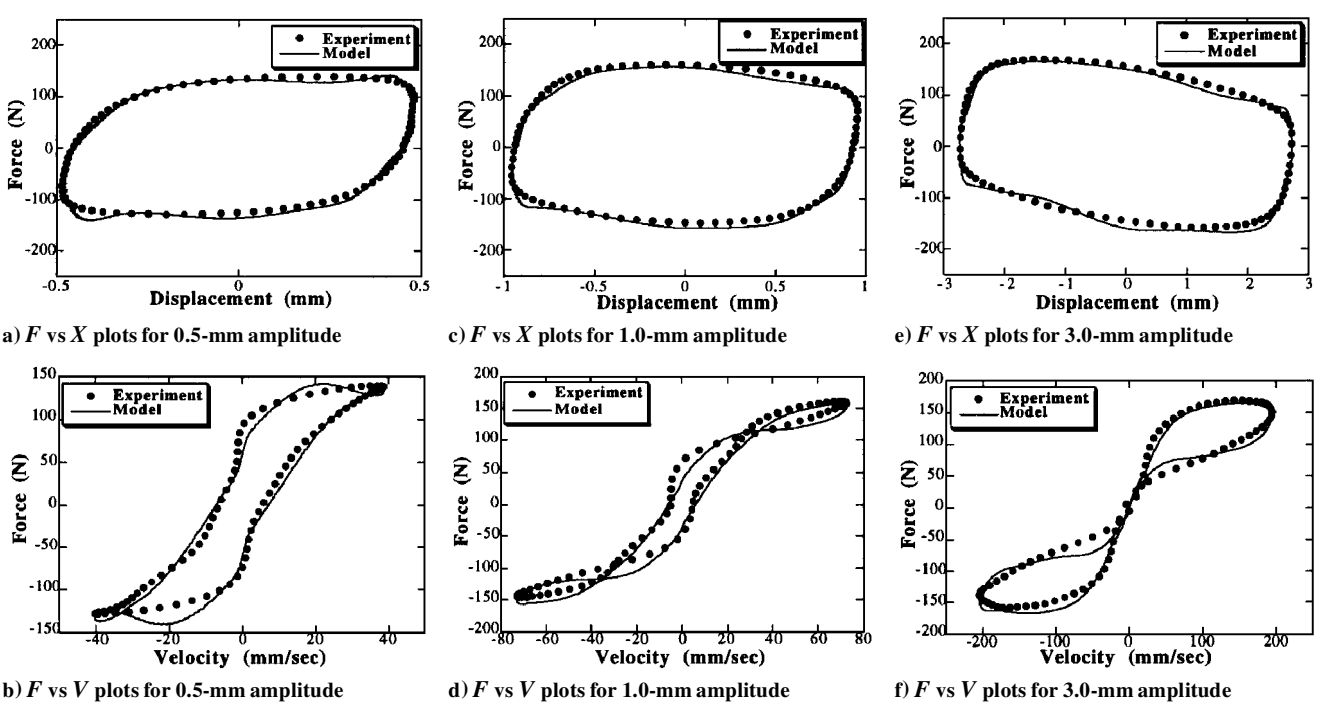

a) F vs X plots for 0.5-mm amplitude
c) F vs X plots for 1.0-mm amplitude
e) F vs X plots for 3.0-mm amplitude
b) F vs V plots for 0.5-mm amplitude
d) F vs V plots for 1.0-mm amplitude
f) F vs V plots for 3.0-mm amplitude

Fig. 11 Comparison of hysteresis cycles from estimated parameters with experimental hysteresis data for $E = 3$ kV/mm.

Table 1 Parameters and objective function values for two nominal data sets using the four-parameter viscoelastic–plastic model and the augmented six-parameter model

	Case 1, $E = 0$ kV/mm, $X_0 = 0.5$ mm		Case 2, $E = 3$ kV/mm, $X_0 = 1.0$ mm	
Parameters	Four-parameter model	Augmented model	Four-parameter model	Augmented model
C_1, N · s/m	3.102*e*3	0.785*e*3	1.093*e*4	0.978*e*4
C_2, N · s/m	2.025*e*4	0.863*e*4	1.111*e*4	1.253*e*4
K_1, N/m	1.240*e*5	1.014*e*5	1.333*e*5	1.453*e*5
C_v, N · s/m	0.900*e*3	2.426*e*3	1.928*e*3	1.914*e*3
R, N · s^2/m	——	0.000	——	5.292
F_c, N	——	20.83	——	4.810
α_y	0.95	0.95	0.40	0.40
ϵ_y	0.10	0.10	0.10	0.10
ϵ_c	——	0.10	——	0.30
J	5.378*e*4	5.814*e*4	1.814*e*5	1.029*e*5

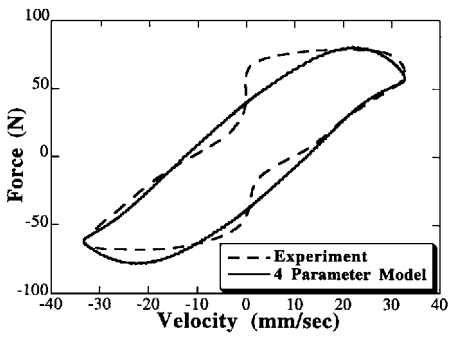

a) Four-parameter viscoelastic–plastic model

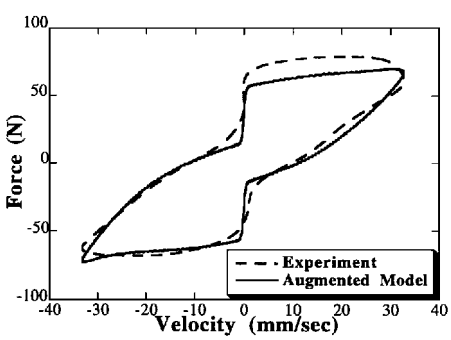

b) Augmented six-parameter model

Fig. 12 Comparison of experimental hysteresis data for $E = 0$ kV/mm, $X_0 = 0.5$ mm, with the model hysteresis plots.

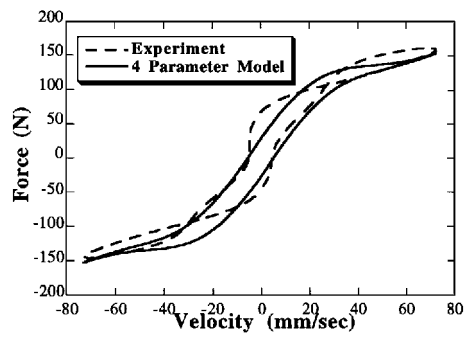

a) Four-parameter viscoelastic–plastic model

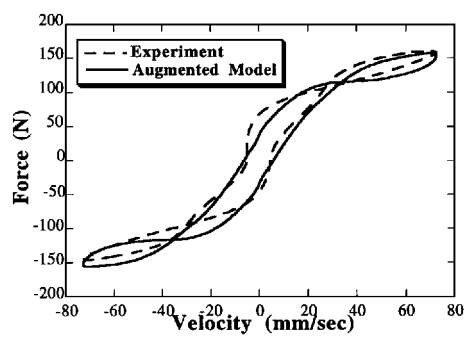

b) Augmented six-parameter model

Fig. 13 Comparison of experimental hysteresis data for $E = 3$ kV/mm, $X_0 = 1.0$ mm, with the model hysteresis plots.

To emphasize the importance of the stiction and inertial parameters that have been included in this model, the force vs velocity plots generated using the augmented six-parameter model are compared with those generated using the four-parameter viscoelastic–plastic model presented in Refs. 23 and 24. Two nominal cases are presented in Figs. 12 and 13. Results for case 1, which corresponds to a preyield condition, are shown in Fig. 12 for an applied field, $E = 0$ kV/mm, and a displacement amplitude, $X_0 = 0.5$ mm. Case 2, which corresponds to a postyield condition (shown in Fig. 13) represents results for an applied field of 3 kV/mm and a displacement amplitude of 1.0 mm. Cases 1 and 2 have been chosen to highlight the effects of stiction and fluid inertia, respectively. The corresponding model parameters for each case are in Table 1. In case 1, the inertial parameter R is estimated to be zero, so that the stiction effects are easily isolated. Although the objective function value for the augmented model is slightly higher than for the four-parameter viscoelastic plastic model from Refs. 23 and 24, Fig. 12b shows a qualitatively better correlation with the experimental data as compared to Fig. 12a. Case 2 shows that the augmented six-parameter model captures the inertial effects as manifested by the loops at the extremities of the hysteresis cycles seen in Fig. 13b. Figure 13a shows a distinct absence of these loops. Moreover, the objective error function decreases in the case of the augmented six-parameter model as seen in Table 1. The model parameters in case 2 do not change significantly between the two models, in spite of adding two parameters. This signifies that the stiction effects are not significant enough at higher amplitudes and that the inertial parameter mainly adds the loops but the outer envelope of the force vs velocity cycle essentially remains the same. However, in case 1, the model parameters vary considerably between the two models.

The additional stiction and inertial parameters do not affect the correlation of the model with the experimental force vs displacement hysteresis data as significantly as for the force vs velocity hysteresis cycles. The four-parameter viscoelastic–plastic model is sufficient to accurately capture the force vs displacement hysteresis cycles and, hence, deduce the energy dissipation of the damper. Thus, if the amount of damping is the important criterion, then the four-parameter viscoelastic–plastic model should give a good estimate. But if the force vs velocity hysteresis behavior is important for predicting system behavior, then the augmented six-parameter model would provide a better prediction.

V. Conclusions

A detailed experimental study of a mixed mode moving electrode ER damper is presented. The hysteresis data clearly describe the damper behavior for different displacement amplitudes and varying

electric field. The stiction effects are important for low amplitudes when the fluid is in the preyield phase. For large amplitudes, the fluid is in the postyield phase and the inertial factors become more important. However, it is difficult to say how much of the observed behavior can be attributed solely to the fluid and how much to the various damper components such as bearings and rod seals. An augmented six-parameter model for the ER damper is proposed that derives its structure solely from the phenomenology of the force vs displacement and force vs velocity hysteresis characteristics as observed from experiments. The model faithfully captures the damper behavior for different field strengths and displacement amplitudes.

This model represents an important aspect for modeling of various dynamic systems such as aircraft landing gears, isolation mounts, and helicopter lag mode damping systems in which ER and MR (magnetorheological) dampers may be implemented. In helicopter rotor systems, stability is very sensitive to the amount of damping in the lag mode. Thus, to evaluate rotor systems with active or semiactive damping systems such as those with ER and MR fluids, an accurate model is needed that is simple enough to be easily incorporated into comprehensive rotor codes. The use of mechanical analogs in the model presented makes it amenable to codes such as UMARC. The simplicity of the model also offers advantages in terms of controlling devices incorporating ER and MR materials. Moreover, because the modeling strategy has been adopted strictly based on the experimentally observed behavior and with a qualitative knowledge of the material properties, this modeling approach can also be applied to MR fluid devices and, in general, to other active and semiactive materials and systems.

Acknowledgments

This work is supported by the U.S. Army Research Office under the Smart Structures University Research Initiative, Contract DAAL03-92-G-0121, with Gary Anderson serving as Contract Monitor.

References

[1]Chopra, I., "Perspectives in Aeromechanical Stability of Helicopter Rotors," *Vertica*, Vol. 14, No. 4, 1990, pp. 457–508.

[2]Felker, F. F., Lau, B. H., McLaughlin, S., and Johnson, W., "Nonlinear Behavior of an Elastomeric Lag Damper Undergoing Dual-Frequency Motion and its Effect on Rotor Dynamics," *Journal of the American Helicopter Society*, Vol. 34, No. 4, 1987, pp. 45–53.

[3]McGuire, D. P., "Fluidlastic Dampers and Isolators for Vibration Control in Helicopters," 50th Annual Forum of American Helicopter Society, Washington, DC, May 1994.

[4]Panda, B., and Mychalowycz, E., "Aeroelastic Stability Wind Tunnel Testing with Analytical Correlation of the Comanche Bearingless Main Rotor," 52nd Annual Forum of American Helicopter Society, Washington, DC, June 1996.

[5]Bir, G., Chopra, I., Ganguli, R., Smith, E. C., Vellaichamy, S., Wang, J., Kim, K. C., Chan, W. Y., Nixon, M. W., Kimata, N. W., Smith, J. A., Torok, M., and Nguyen, K., "University of Maryland Advanced Rotorcraft Code (UMARC) Theory Manual," Univ. of Maryland, UM-AERO Rept. 94-18, College Park, MD, July 1994.

[6]Stanway, R., Sproston, J. L., and El-Wahed, A. K., "Application of Electro-Rheological Fluids in Vibration Control: a Survey," *Smart Materials and Structures*, Vol. 5, No. 4, 1996, pp. 464–482.

[7]Brooks, D. A., "Design and Development of Flow Based Electro-Rheological Devices," *International Journal of Modern Physics B*, Vol. 6, Aug. 1992, pp. 2705–2730.

[8]Duclos, T. G., "Design of Devices Using Electrorheological Fluids," *Society of Automotive Engineering Transactions*, Vol. 97, Sec. 2, Paper 881134, 1988, pp. 2.532–2.536.

[9]Carlson, J. D., Catanzarite, D. M., and St.Clair, K. A., "Commercial Magneto-Rheological Fluid Devices," *Proceedings of the 5th International Conference on Electro-Rheological, Magneto-Rheological Suspensions and Associated Technology* (Sheffield, England, UK), World Scientific, Rivers Edge, NJ, 1995, pp. 20–28.

[10]Weiss, K. D., Carlson, J. D., and Nixon, D. A., "Viscoelastic Properties of Magneto- and Electro-Rheological Fluids," *Journal of Intelligent Material Systems and Structures*, Vol. 5, Nov. 1994, pp. 772–775.

[11]Kamath, G. M., Hurt, M. K., and Wereley, N. M., "Analysis and Testing of Bingham Plastic Behavior in Semi-Active Electrorheological Fluid Dampers," *Smart Materials and Structures*, Vol. 5, No. 5, 1996, pp. 576–590.

[12]Gavin, H. P., Hanson, R. D., and Filisko, F. E., "Electrorheological Dampers, Part I: Analysis and Design," *Journal of Applied Mechanics*, Vol. 63, Sept. 1996, pp. 669–675.

[13]Gavin, H. P., Hanson, R. D., and Filisko, F. E., "Electrorheological Dampers, Part II: Testing and Modeling," *Journal of Applied Mechanics*, Vol. 63, Sept. 1996, pp. 676–682.

[14]Gamota, D. R., Wineman, A. S., and Filisko, F. E., "Fourier Transform Analysis: Nonlinear Dynamic Response of an Electrorheological Material," *Journal of Rheology*, Vol. 37, No. 5, 1993, pp. 919–933.

[15]Gamota, D. R., and Filisko, F. E., "Dynamic Mechanical Studies of Electro-Rheological Materials: Moderate Frequencies," *Journal of Rheology*, Vol. 35, No. 3, 1991, pp. 399–425.

[16]Gamota, D. R., and Filisko, F. E., "High Frequency Dynamic Mechanical Study of an Aluminosilicate Electrorheological Material," *Journal of Rheology*, Vol. 35, No. 7, 1991, pp. 1411–1426.

[17]Kamath, G. M., and Wereley, N. M., "Distributed Damping of Rotorcraft Flexbeams Using Electrorheological Fluids," *AIAA Adaptive Structures Forum* (New Orleans, LA), AIAA, Washington, DC, 1995, pp. 300–325.

[18]Kamath, G. M., and Wereley, N. M., "A Nonlinear Viscoelastic-Plastic Model for Electrorheological Fluids," *Smart Materials and Structures*, Vol. 6, No. 3, 1997, pp. 351–359.

[19]Stanway, R., Sproston, J., and Stevens, N. G., "Non-Linear Modelling of an Electrorheological Vibration Damper," *Journal of Electrostatics*, Vol. 20, No. 2, 1987, pp. 167–184.

[20]Ehrgott, R. C., and Masri, S. F., "Modelling the Oscillatory Dynamic Behavior of Electrorheological Materials," *Smart Materials and Structures*, Vol. 1, No. 4, 1992, pp. 275–285.

[21]Lou, Z., Ervin, R. D., and Filisko, F. E., "A Preliminary Parametric Study of Electrorheological Dampers," *Electro-Rheological Flows*, ASME FED–Vol. 164, American Society of Mechanical Engineers, New York, 1993, pp. 143–156.

[22]Spencer, B. F., Dyke, S. J., Sain, M. K., and Carlson, J. D., "Phenomenological Model of a Magnetorheological Damper," *Journal of Engineering Mechanics*, Vol. 123, No. 3, 1997, pp. 230–238.

[23]Kamath, G. M., and Wereley, N. M., "System Identification of ER Fluid Dampers Using a Nonlinear Mechanisms-Based Model," *Proceedings of the 1996 SPIE Conference on Smart Structures and Materials* (San Diego, CA), Society of Photo-Optical Instrumentation Engineers, 1996 (SPIE Paper 2717-46).

[24]Kamath, G. M., and Wereley, N .M., "Modeling the Damping Mechanism in ER Fluid Based Dampers," *M3DIII: Mechanics and Mechanisms of Material Damping*, edited by V. K. Kinra and A. Wolfenden, American Society for Testing and Materials, 1997, pp. 331–348 (STP 1304).

[25]Makris, N., Burton, S. A., Hill, D., and Jordan, M., "Analysis and Design of ER Damper for Seismic Protection of Structures," *Journal of Engineering Mechanics*, Vol. 122, No. 10, 1996, pp. 1003–1011.

[26]Vanderplaats, G. N., and Hansen, S. R., "DOT Users Manual," Version 2.04B, VMA Engineering, Goleta, CA, 1990.